Enhanced mixing and spatial instability in concentrated bacterial suspensions

Andrey Sokolov,[1,2] Raymond E. Goldstein,[3] Felix I. Feldchtein,[4] and Igor S. Aranson[1]

[1]*Argonne National Laboratory, 9700 South Cass Avenue, Argonne, Illinois 60439, USA*
[2]*Illinois Institute of Technology, 3101 South Dearborn Street, Chicago, Illinois 60616, USA*
[3]*Department of Applied Mathematics and Theoretical Physics, University of Cambridge, Wilberforce Road, Cambridge CB3 0WA, United Kingdom*
[4]*Imalux Corporation, 1771 East 30th Street, Cleveland, Ohio 44114, USA*

High-resolution optical coherence tomography is used to study the onset of a large-scale convective motion in free-standing thin films of adjustable thickness containing suspensions of swimming aerobic bacteria. Clear evidence is found that beyond a threshold film thickness there exists a transition from quasi-two-dimensional collective swimming to three-dimensional turbulent behavior. The latter state, qualitatively different from bioconvection in dilute bacterial suspensions, is characterized by enhanced diffusivities of oxygen and bacteria. These results emphasize the impact of self-organized bacterial locomotion on the onset of three-dimensional dynamics, and suggest key ingredients necessary to extend standard models of bioconvection to incorporate effects of large-scale collective motion.

PACS number(s): 87.18.Fx, 87.16.−b, 05.65.+b

I. INTRODUCTION

Physical mechanisms governing large-scale organization of self-propelled biological microparticles, such as motor proteins, swimming bacteria, and other motile cells, significant attention among physicists and biologists [1,2]. Colonies of self-propelled micro-organisms often exhibit collective behavior including swarms and vortices, absent from passive systems, such as suspensions of inert particles. The collective behavior of motile aerobic bacteria, especially at high concentrations, is governed by a subtle interplay between buoyancy, hydrodynamic interactions, oxygen consumption, and mixing [3–10]. A recent consensus is that emergent dynamic behavior and self-organization in suspensions of swimming bacteria can arise through hydrodynamic interactions between the organisms [5,6,10]. Large-scale self-organization is driven by the input, into the surrounding fluid, of mechanical energy from the organisms' rotating flagella. It returns from the fluid into the ensemble of swimmers, thus, cascading from the smallest scales to the largest that greatly exceed the size of individual organisms. Studies of concentrated bacterial suspensions help reveal the physical and biological mechanisms governing behavior of bacterial colonies near air/water interfaces, where oxygen-driven self-concentration of bacteria may occur near contact lines [6]. In addition, such flows are important for fundamental and technological reasons, from understanding coherent motion in groups of interacting objects (flocks, schools, and herds [11–13]) to microfluidic devices such as bacteria-powered micromixers [14].

Aerobic bacteria, such as *Bacillus subtilis*, often develop spatial patterns through a different physical mechanism, *bioconvection* [4], which occurs in fluid domains open to the air above, whose dissolved oxygen is consumed by the suspended bacteria and replenished from the air-water interface. This leads to an oxygen gradient that drives chemotaxis of bacteria upward, producing a depletion zone in the bulk of the suspension and accumulation at the free surface. As the bacteria are slightly denser than water, this is an unstable arrangement resulting in large-scale circulation (or convection). Such convective motion can enhance mixing within the fluid [6].

The possible biological advantage of self-organization relative to random swimming motions and the relationship between collective motion and bioconvection are two important questions in current studies of these systems. To address these, we have performed a series of experiments on free-standing liquid films of concentrated suspensions of *Bacillus subtilis*. The features of these experiments include accurate control of the film thickness and the bacterial concentration during the experiment and use of the noninvasive technique of optical coherence tomography (OCT) to image bacterial dynamics in the *bulk* of the film. Our observations show that the quasi-two-dimensional (2D) collective swimming state observed at high micro-organism concentration in pendant drops [5] and thin films [10] loses its stability and gives rise to a "turbulent" three-dimensional (3D) state. We find that the three-dimensional circulatory motion appears at much lower film thicknesses than would be predicted by the accepted models of buoyancy-driven bioconvection [15]: the three-dimensional behavior appears at a "bioconvection Rayleigh" number that is roughly two orders of magnitude lower than that predicted by a linear stability analysis of the stationary state [15]. Our space- and time-resolved experiments point to a different criterion: in the presence of collective motion, the three-dimensional circulation coincides with the onset of an oxygen depletion layer in the middle of the film.

Moreover, we show that it is possible to characterize the observed properties of the collective state by effective transport coefficients for diffusion of oxygen and bacteria, increased by up to two orders of magnitude relative to the dilute limit. Thus, our experimental results emphasize the ultimate role of self-organized collective motion on the onset of large-scale three-dimensional circulation in concentrated bacterial suspensions. In turn, since this circulation enhances mixing and transport of oxygen by at least an order of magnitude, the self-organized motion may be advantageous for
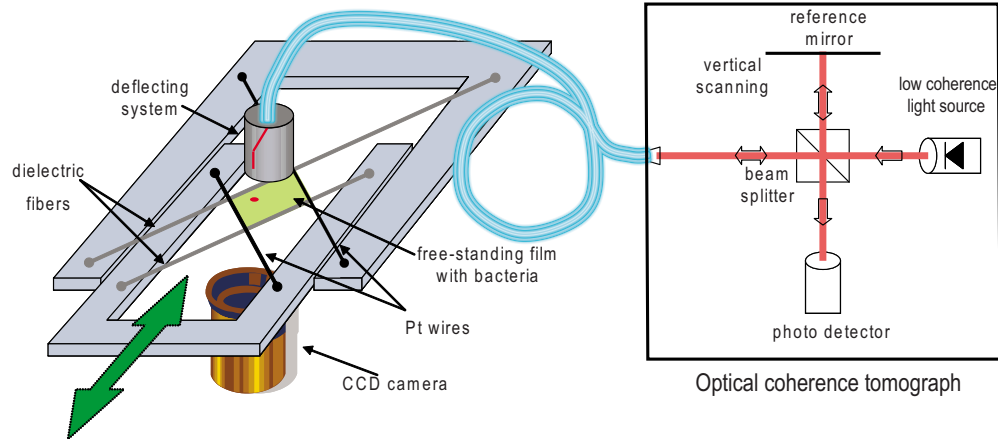
FIG. 1. (Color online) Schematic of the experimental apparatus. A thin liquid film containing bacteria spans two adjustable Pt wires and two dielectric fibers and is stretched by a movable platform controlled by a stepper motor. Bright-field images of the bottom surface of the film are obtained by a long working distance microscope objective mounted under the film and recorded by a high-speed charge-coupled device (CCD) camera (Spot Boost EMCCD 2100, Diagnostic Instruments Inc.). To obtain the local concentration of bacteria in the bulk of the film, we used a high-resolution, noninvasive, and optical coherence tomography to measure the profile of the optical scattering (which is approximately proportional to the bacterial concentration). From this, cross-sectional images were created by scanning the beam position laterally over the film or by horizontal displacement of the microscope platform with respect to OCT probe.

the population. By analogy with the concept of "turbulent viscosity" in the theory of hydrodynamic turbulence, where chaotic motion of the fluid is incorporated by an increased viscous dissipation [16], we show that is possible to capture both qualitatively and quantitatively the experimental results within standard models of oxygentaxis, developed for the dilute case, with effective transport coefficients increased by roughly two orders of magnitude.

We suggest that the reason behind such agreement between experiment and this simplified theory is the existence of a well-defined spatial scale in the collective dynamics of bacteria, in contrast to the case of hydrodynamic turbulence. Consequently, the "turbulent diffusivity" is defined as a product of characteristic length scale and typical velocity, both of which are well-defined for the self-organized swimming state (see, e.g., [10]). In hydrodynamic turbulence, there is no well-defined scale of velocity, and—as a result— the "turbulent velocity" is not uniquely defined.

In Sec. II of this paper, we discuss experimental materials and methods followed by a presentation of experimental results in Sec. III. The value of diffusion coefficients obtained from the concentration profiles in the bulk of the film is compared with well-established models of bioconvection. Steady-state concentration profiles are considered in Sec. IV.

II. MATERIALS AND METHODS

Experiments were conducted on suspensions of *B. subtilis* strain 1085, a peritrichously flagellated rod-shaped bacterium ~ 4 μm long and ~ 0.7 μm in diameter. Bacteria were grown in Terrific Broth (TB) medium (Sigma T5574), washed, and then concentrated by centrifugation. In a typical experiment, the average concentration of bacteria was $\sim 2 \times 10^{10}$ cm^{-3}, which is approximately 20-fold higher than in the stationary growth phase of *B. subtilis*. Yet, it is important to recognize that in self-concentration of bacteria in small

droplets near water/air contact lines (see Ref. [6]), such high concentrations can be achieved in small volumes under laboratory conditions even without centrifuging.

The experimental setup is shown in Fig. 1. A small drop of bacterial suspension is placed between two supporting crossed pairs of fibers: two platinum (Pt) wires and two dielectric fibers forming a small square window. The drop was stretched to the necessary thickness by a computer-controlled stepper motor that moves a supporting platform attached to one crossed pair of the fibers. To determine in real time the area of the film, and, correspondingly, the film thickness, the arm of sliding rheostat was mechanically connected to the movable platform. The area of the film was established from the rheostat's resistance, following suitable calibration procedure. A custom control program within LABVIEW (National Instruments) allowed the window size to be adjusted from 1 to 10 mm with an accuracy of ± 20 μm. The corresponding thickness of the liquid film ranged from 1 μm to 1 mm. Film thickness was measured either indirectly (from the initial volume of the droplet and the area of the film) or directly by OCT scanning. The experimental cell was placed in a humidity-controlled chamber to reduce evaporation.

The three-dimensional bacterial concentration distribution was probed noninvasively by high-resolution OCT [17], an interferometric technique for imaging in scattering media. It measures an over the depth profile of optical scattering using light of low coherence and then creates a cross-sectional image by scanning the beam position laterally over the sample. The technique of OCT is based on the fact that as light propagates in a scattering medium, only the reflected (non-scattered) light is coherent. Thus, an optical interferometer can be used to detect only coherent light and to separate scattered light. Our experiments used a commercially available imaging system (Niris OCT, Imalux Corporation, Cleveland, OH). The time domain OCT system [18] uses common path optical topology, a 1310-nm-central wavelength with 55 nm bandwidth. It has in-depth resolution of 15 μm in free
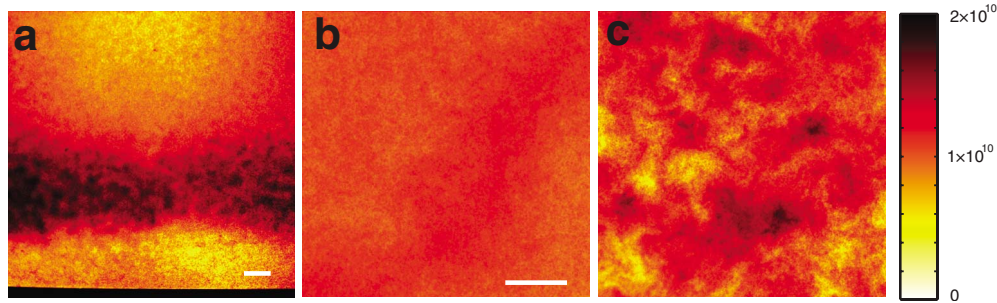
FIG. 2. (Color online) (a) Pseudocolor representation of formation of spots in a type-I experiment during the migration of cells from the electrode, seen as black strip on the bottom (scale bar 200 μm). Color bar on the right indicates values of mean concentration $\bar{n}$ in cells/cm^3. See also movies 1 and 2 [20]. (b) and (c) Formation of spots after the thickness of the film was suddenly increased, using type-II technique. Initially uniform concentration of bacteria (2 s elapsed) (b); final stage after 60 s (c).

space, 11 μm in water, with a 1.5 s acquisition time for an image of maximal resolution up to 200×200 pixels. The OCT probe has a diameter of 2.7 mm and a 2-mm-lateral field of view, with 25 μm lateral resolution, and can be easily mounted in close proximity to the sample film to image its full depth (about 1 to 2 mm above the film). The lateral OCT scan is performed either by moving the sample or the probe beam illuminating the sample, while the OCT depth scan is performed by the piezofiber delay line.

A. Concentration calibration

To perform a calibration of signal versus concentration, we measured the brightness of the OCT image from liquid films with uniformly distributed dead (nonmotile) *B. subtilis* killed by a small drop of alcohol. The suspension of dead bacteria was split to five 1.5 ml plastic tubes. After centrifugation, the liquid from tubes was removed and the net weight of bacteria in each tube was measured with the precision of ± 0.5 mg ($\approx 3\%$ of typical weight). Since the bacterial body is approximately a spherocylinder with aspect ratio ≈ 7 and the volume fraction of randomly dense-packed spherocylinders of the same aspect ratio is ≈ 0.5 (see [19]), we can estimate the net weight of bacteria as a half of measured weight after centrifuging. The number of bacteria was estimated from an assumption that the average bacteria weight is 2.5×10^{-12} g. To prepare suspensions with five known concentrations of bacteria, an appropriate amount of liquid was added to each tube. Our measurements show that in the range of concentrations under consideration, $n \lesssim 3 \times 10^{10}$ cells/cm^3, the brightness of the OCT image is a nearly linear function of the concentration, implying that these five calibration points are sufficient for accurate concentration estimates. Interpolation was used to extend these results to the whole set of concentrations.

B. Experimental protocols

Two complementary protocols were used to perform experiments with variable concentration of bacteria. In "type-I" experiments, the bacteria are concentrated by transmission of a small electric current between the platinum wires [10]. A dc voltage of 2.4 V applied between the Pt wires creates electrolysis, resulting in a change in pH near the wires. This

triggers a chemotactic response; the bacteria tend to swim away from the electrodes toward the middle of the cell [Fig. 2(a)]. The ions produced near the electrodes slowly diffuse to the center of the window and thereby force bacteria to concentrate into a thin strip. The concentration of bacteria inside this strip can be up to five times larger than the mean. In "type-II" experiments, the thickness of the film is suddenly increased from 50 to 400 μm by a rapid compression of the area of the film [Figs. 2(b) and 2(c)]. While the type-I technique allows for a gradual increase in the bacterial concentration in the middle of the experimental cell, the type-II method allows resetting the bacterial concentration distribution to near uniformity across the entire film.

III. EXPERIMENTAL RESULTS

In a previous work [10] with *B. subtilis* in a monolayer-thick film, we found that when the bacterial surface coverage exceeds ~30% (corresponding to volume concentration $\bar{n} \approx 10^{10}$ cells/cm^3), hydrodynamic interactions between swimming cells result in a large-scale collective motion with a typical speed $V_0 \sim 50$–100 μm/s and characteristic length $L_0 \sim 50$ μm. Here we focus on the effects of increased film thickness and bacterial concentration.

Both type-I and type-II experiments consistently revealed that above a critical film thickness (~200 μm), the spatially homogeneous self-organized bacterial motions transform into a highly inhomogeneous dynamic state characterized by spontaneous formation and dissolution of dense regions, seen as dark spots in Figs. 2(a) and 2(c). [Note that the contrast in these images is digitally enhanced; in raw images, the entire brightness variations are below 30% of the mean.] In particular, in type-II experiments, when the thickness of the film was changed suddenly from 50 to 400 μm, after ~10 s we observed concentration fluctuations whose amplitude increased in time for about 1 min [Fig. 2(c)]. We show below that these dark regions are manifestation of large-scale three-dimensional structures (plumes).

To understand the nature of the spots and their relationship with the film thickness d, we used the type-II protocol to decrease the film thickness by small steps from 600 to 50 μm, measuring for each value of the thickness an average spot size. For each d, a sequence of 30 images obtained
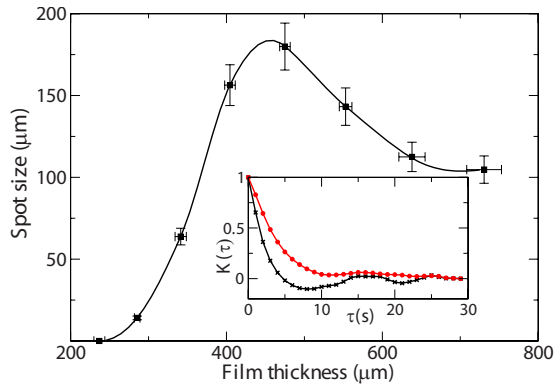
FIG. 3. (Color online) Average spot size vs film thickness d with corresponding error bars. Inset: temporal autocorrelation function of the bacterial concentration averaged over vertical coordinate, for thicknesses of 50 μm (red ●) and 400 μm (black ×).

at $\sim$1 frame per second was processed to accumulate sufficient statistics. As shown in Fig. 3, spots appear above a critical thickness $d_c \approx 200$ μm, with the average spot size reaching a maximum at $d \approx 400$ μm, of approximately half of the film thickness, and then decreasing with further increase in the thickness. Our measurements show that the amplitude of concentration fluctuations in the spots is approximately 30% of the mean.

We have computed the temporal correlation function of the intensity I of light transmitted though the film,

$$K(\tau) = \frac{\langle I(t)I(t+\tau)\rangle - \langle I(t)\rangle^2}{\langle I(t)^2\rangle - \langle I(t)\rangle^2}, \qquad (1)$$

which is related to the concentration of bacteria averaged over a particular vertical cross section. This is determined as a function of time delay τ between frames for every pixel in the frame and averaged over the entire frame area. Figure 3 clearly shows decay of autocorrelation with the characteristic time $\tau \sim 7$ s, thus, defining the typical time scale over which

the spot disappears, flows away, or merges with another spot. This time scale is roughly determined by the ratio of typical spot's size to the speed of collective flows, which is about 50–100 μm/s. However, in contrast to thin films, in thick films we also observed a second peak in the correlation function at approximately 20 s. This time scale, which is the order of time needed for bacteria to traverse the film in vertical direction, is likely a hint to a three-dimensional motion.

To obtain space- and time-resolved data on the local bacterial concentration, we have used OCT. The initial bacterial distribution was made as nearly uniform as possible (either by mixing the suspension or by the rapid change in the area of the film). Selected results are shown in Figs. 4(a) and 4(b). In thin films ($d < 100$ μm), the concentration distribution remains close to uniform with only a slight parabolic depression in the middle of the film. This observed accumulation of aerobic bacteria at open surfaces due to oxygentaxis is distinct from highly localized distributions due to the hydrodynamic attraction of *E. coli* to hard walls recently studied [21]. The characteristic scale of the concentration variation due to hydrodynamic attractions is $\sim$10–15 μm in the vicinity of the wall and about 25–35 μm in the bulk. In contrast, on the scale of our experiments, we did not observe any noticeable concentration increase near solid objects inserted into the film.

As the thickness of the film is increased into the range 100 μm $< d <$ 500 μm, the depletion in the middle of the film and the accumulation at the surfaces take place after approximately $\sim$3 s. This is significantly faster than in earlier studies [5], possibly due to the much higher average concentrations. Figure 4(c) shows a range of concentration profiles as a function of the vertical coordinate z scaled by the total film thickness d. The distributions are nearly symmetric with respect to the layer center. In this regime, the formation of spots occurs; the in-plane concentration distribution becomes significantly nonuniform, which in turn is manifested by growing plume structures in the cross section [Fig. 4(d) and movie 4]. The downward plume's velocity is about 10–20 μm/s. Due to plume's downward motion, the
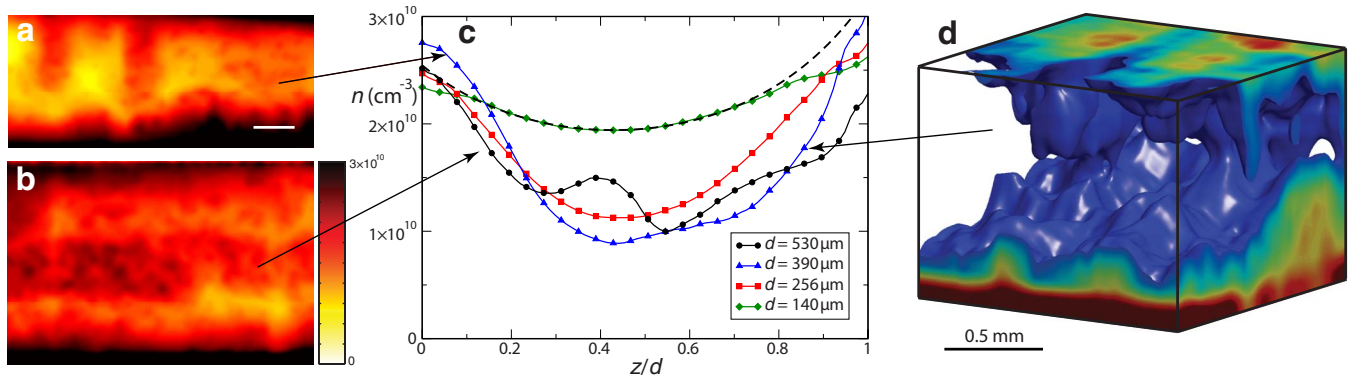

FIG. 4. (Color online) OCT images of bacterial concentration distribution inside film. (a) Formation of falling plumes. (b) Layer of immotile bacteria slowly decays (scale bar 100 μm); see also supplementary movies 3 and 4 [20]. (c) Concentration profile $n(z)$ vs vertical coordinate z for different film thicknesses averaged over film area and time. $z=0$ corresponds to the top surface of the film and $z=d$ to the bottom surface. Error bars are on the order of 5–10 %; instrumental errors are significantly smaller. Dashed line is theoretical prediction (4). (d) Three-dimensional scan of the bacterial concentration n obtained by OCT for $d \approx 500$ μm. The isosurface shown is for $n = \bar{n}/3$, where $\bar{n}$ is average concentration, and the colors indicate concentration distribution (red corresponds to maximum; blue to $n = \bar{n}/3$). See also movie 5 in [20].

bottom layer also becomes engaged into circulation (or convection). For even thicker films ($d > 500$ μm), we have noticed the formation of an additional transient dense layer of immobile bacteria in the middle. This layer composed of bacteria temporarily rendered nonmotile by lack of oxygen appears after $\sim$30 s. The concentration profile has a peak near the middle of the layer [Fig. 4(c), $d = 530$ μm]. This peak slowly migrates to the bottom of the film due to gravity. In this case, we observed a noticeable slowdown of plume motion related to the formation of wide depletion layers.

In additional experiments, we filled the experimental chamber with nitrogen to reduce a concentration of dissolved oxygen in the film. We observed that in the course of filling of the chamber, the intensity of layer's transparency fluctuations decreased leading to a complete disappearance of the spots and essentially uniform distribution of bacteria (see movie 5). These experiments confirm that the formation of spots is related to bacterial motility and oxygentaxis. In an independent experiment [22], we verified that filling of the experimental chamber with nitrogen leads to nearly complete cessation of bacterial motility. For concentrations of bacteria $\sim 2 \times 10^{10}$ cm^{-3}, the time scale associated with the cessation of motility is on the order of 3 s.

A. Enhanced mixing

Measurements of the vertical concentration profiles over a range of film thicknesses provide a unique opportunity to extract effective mixing characteristics of bacterial suspensions, such as the effective translational diffusion constant of bacteria (D_n) and of oxygen (D_c). The very smooth concentration profiles seen in Fig. 4(c) hint at the rather large values of these diffusion coefficients, and, correspondingly, the length scale λ for decay of the concentration away from the surfaces. Values of $D_{c,n}$ can be estimated from the typical velocity of bacteria on the surface of the film V, which is on the order of $V \approx 50$–100 μm/s, and the characteristic length of turbulent motion (mixing length) $L_0 \approx 50$ μm, $D_{c,n} \approx VL_0$ (compare to Taylor dispersion [23]), and in qualitative agreement with previous work by Wu and Libchaber [3].

Alternatively, similar estimates can be obtained by fitting the data to well-established models of oxygen and bacterial dynamics,

$$c_t + \mathbf{u} \cdot \boldsymbol{\nabla} c = D_c \nabla^2 c - kn, \qquad (2)$$

$$n_t + \mathbf{u} \cdot \boldsymbol{\nabla} n = D_n \nabla^2 n - \boldsymbol{\nabla} \cdot [\mu n \boldsymbol{\nabla} c]. \qquad (3)$$

These equations are valid when there is no fluid flow due to self-organized bacterial swimming, i.e., for the relatively dilute case. For high bacterial concentration, one must extend the corresponding (Navier)-Stokes equation for the hydrodynamic velocity $\mathbf{u}$ by a coarse-grained stress tensor accounting for the active motion of hard inclusions in fluid (see for the discussion in Refs. [8,24]). Here $\mathbf{u}$ is the fluid velocity; $k \approx 10^6$ molecules/cell/s is the oxygen consumption rate. Under normal conditions (no collective swimming), the estimates for the diffusivity of bacteria are $D_n \approx D_{n0} \approx 1.3 \times 10^{-6}$ cm^2/s, and the oxygen diffusion constant for low concentration of cells is estimated to be $D_c \approx D_{c0} \approx 2.1$

TABLE I. The length λ and the enhancement factor $\zeta = D_c D_n / D_{c0} D_{n0}$ for four different values of the film thickness d. The last column indicates the type of flow: 2D–no circulation, 3D–three-dimensional circulatory motion.

Thickness d (μm)	Length λ (μm)	$\zeta = D_c D_n / D_{c0} D_{n0}$	–
140	120	144	2D
256	114	130	2D
390	180	324	3D
520	340	1156	3D

$\times 10^{-5}$ cm^2/s [15]. The chemotactic sensitivity μ is on the order of 10^{-21} cm^5/s [6].

In the absence of an explicit velocity field, Eqs. (2) and (3) yield the steady-state concentration profile that is of the form (see also Sec. IV)

$$n = n_0 \sec^2 \left[\sqrt{\frac{\mu k n_0}{2 D_n D_c}} (z - z_0) \right], \qquad (4)$$

where the constant $z_0 \approx d/2$ and n_0 is the concentration in the middle of the film, $z = z_0$.

The comparison shows that the experimental concentration profile in Fig. 4(c) for $d = 140$ μm matches well to theoretical prediction (4) (dashed line) with $\lambda \approx 110$ μm and $D_c D_n \approx 10^{-9}$ cm^4/s^2, which is $\sim$100 times larger than the expected value of 10^{-11} cm^4/s^2 [6]. Roughly, the same values are obtained assuming that $D_c \approx D_n \approx VL_0 = 2.5$–$5 \times 10^{-5}$ cm^2/s, giving $D_c D_n = 0.6$–2.5×10^{-9} cm^4/s^2. The results of this analysis are summarized in Table I. We see that the extracted diffusion coefficients D_c and D_n exceed the anticipated diffusivities for dilute suspensions of bacteria D_{c0}, D_{n0} at least by the order of magnitude, depending on the film thickness. Moreover, our results clearly show that large-scale convection motion leads to further increase in the enhancement factor $D_c D_n / D_{c0} D_{n0}$.

We comment here that while Eqs. (2) and (3) are formally valid only for dilute suspensions, their functional form, expressing the conservation of number of bacteria and advection flux in the direction of chemical gradient, is more general. It justifies this simple description of transport and mixing by increased diffusion coefficients.

B. Bioconvection threshold

A linear stability analysis [15] of stationary concentration distributions $n(z)$ in the framework of Eqs. (2) and (3) shows that the stability criterion for the onset of bioconvection is determined by

$$\Gamma = \frac{v_0 \alpha \bar{n} g h^3}{\nu D_n}, \qquad (5)$$

the analog of the Rayleigh number in thermal convection, and by the Schmidt number $\mathrm{Sc} = \nu / D_n$. Here, $\bar{n}$ is average cell concentration, $v_0 \approx 1$–2×10^{-12} cm^3 is the bacterium volume, $\alpha \approx 0.1$ is the relative bacteria/water density difference, $g = 980$ cm/s^2 is the gravitational acceleration, ν
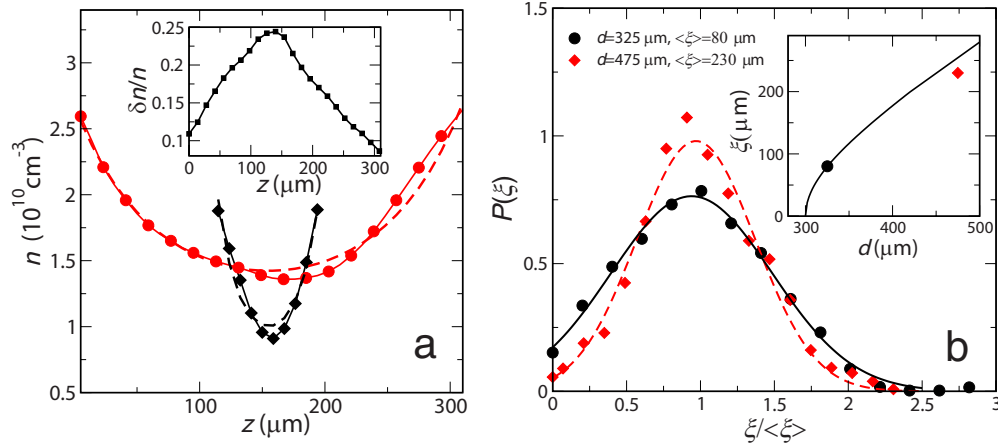
FIG. 5. (Color online) Bacterial concentration. (a) Vertical profiles of bacteria concentration average over 600 vertical scans (red line with circles) and in the depletion layer only (black line with diamonds) for $\bar{n} \approx 1.8 \times 10^{10}$ cm^{-3}. Correspondingly, $\lambda \approx 200$ μm in the film and $\lambda \approx 50$ μm in the depletion layer; dashed lines are fits to Eq. (4). Inset: relative standard deviation of concentration $\delta n/n$ vs z. Inset also provides error bars for $n(z)$ profiles in (a). (b) Probability distribution $P(\xi)$ for the width of depletion layer ξ for $d \approx 325$ μm film (circles) and $d \approx 475$ μm (diamonds). Lines show fits to the Gaussian law $P(\xi) \sim \exp[-(\xi - \langle \xi \rangle)^2/\sigma^2]$. Inset: depletion layer thickness ξ vs d obtained from theoretical model. Symbols depict corresponding experimental results.

$=0.01$ cm^2/s is water's kinematic viscosity, and $h = d/2$ is half-thickness of the film (since both top and bottom surfaces of our film are exposed to oxygen). For the parameters of our experiment, $\bar{n} \approx 2 \times 10^{10}$ cm^{-3}, $D_n \sim V L_0 \approx 0.3 - 0.5 \times 10^{-4}$ cm^2/s, and the convection is observed for the half-thickness $d/2 = 150$ μm. It yields the following values: Sc ≈ 300 and $\Gamma \approx 10$. For the same conditions, Ref. [15] reports the threshold value of $\Gamma \approx 600 - 700$, roughly two orders of magnitude higher. Thus, our measurements rule out traditional mechanism for the onset of bioconvection in the presence of large-scale collective motion.

C. Analysis of fluctuations in the depletion layer

Our results show that the three-dimensional instability and formation of plumes are closely related to the onset of a depletion zone, the region in which the concentration of bacteria is significantly lower than the average due to oxygen-taxis toward the surface of the film. Near free surfaces, concentrated bacteria produce large-scale motion with an average in-plane speed $V_0 \approx 50 - 100$ μm/s, making the effective diffusion coefficients much higher than at the low concentration found inside depletion layer. We conclude that the plumes arise from the *intrinsic* fluctuations of concentration and velocity due to the self-organized large-scale motion of bacteria. Once a dense domain of bacteria falls into the depletion zone due random fluctuations of the depletion layer interface, it continues to fall since the bacteria become temporally nonmotile by the lack of dissolved oxygen. In support of this observation, we quantify the fluctuations at the depletion layer interface. We plot separately the vertical concentration profile inside the depletion layer and averaged over the entire film in Fig. 5(a). By fitting experimental data to Eq. (4), we extract the length λ and corresponding diffusions coefficients in both regions. We find that inside the depletion layer, the diffusivity D_n is closer to that of dilute suspensions, i.e., $D_n \approx 5 \times 10^{-6}$ cm^2/s. The fluctuation-induced mechanism of plume generation at the interface of the depletion layer is also supported by the analysis of the standard deviation δn at various vertical positions z inside the film [inset to Fig. 5(a)]. One sees that fluctuations are minimal at the top and the bottom surface of the film and increase significantly in the middle of the film where the depletion layer is located.

Our OTC measurements show that the depletion layer thickness ξ fluctuates around an average value that depends on the film thickness d. The probability distribution of the width ξ scaled on the average value $\langle \xi \rangle$ is shown in Fig. 5(b). The locations of the depletion layer were determined from the threshold concentration n_{th} where bacteria experience motility loss due to lack of oxygen. For our experimental conditions, we find $n_{th} \approx \bar{n}/2$. The distribution functions $P(\xi)$ are consistent with a Gaussian law, which can be anticipated from the assumption that the boundaries of the depletion layer exhibit random fluctuations. For the film thickness $d = 325$ μm, we obtained an average thickness of the depletion layer $\xi \approx 80$ μm and standard deviation $\sigma = 43$ μm. For the thicker films, $d = 475$ μm, we find $\xi \approx 230$ μm and $\sigma = 92$ μm. These experimental results are in good agreement with theoretical prediction [see Eq. (7) below] for the concentration $\bar{n} \approx 2 \times 10^{10}$ cm^{-3}. The depletion layer appears if $d > 280$ μm.

Figure 6(a) shows the vertical concentration profiles in different regions in the regime of well-developed three-dimensional motion, corresponding to the case when the concentration profile averaged over the entire film is almost parabolic [Fig. 5(a)]. As one sees from Fig. 6(a), the concentration profiles show very strong variations, especially when the plumes are formed. To characterize these variations, we determined the 2D probability distribution $P(n, z)$ for concentration of bacteria and distance from the top surface of the film z. As one sees from Fig. 6(b), $P(n, z)$ has a significant broadening around the mean profile $\langle n(z) \rangle$ due to the chaotic motion of plumes and fluctuations of the depletion layer position.
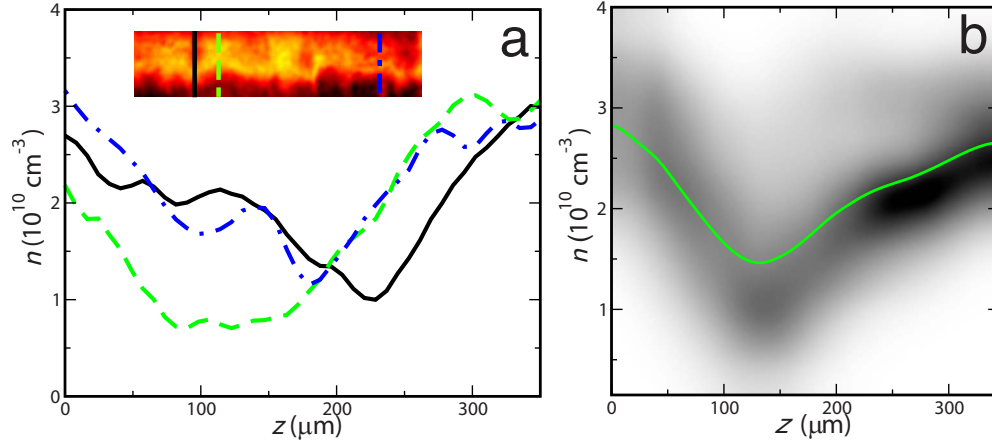
FIG. 6. (Color online) Plumes. (a) Vertical concentration profiles in the plume (solid black line), in the vicinity of the plume (dashed green line), and near the potential location of plume formation (point-dashed blue line). (b) Grayscale representation of 2D probability distribution $P(n,z)$ for the concentration of bacteria n and coordinate inside the film z, where black corresponds to higher probability. 25 sample points for concentration $\times 25$ points for thickness used, then smoothed. Average concentration $\bar{n}$ is 2.2×10^{10} cm^{-3}. Solid line depicts the mean concentration profile $\langle n(z) \rangle$.

Thus, our measurements support the interpretation that the fluctuations, which originated from the intrinsic chaotic nature of the collective motion, are amplified due to the formation of the depletion layer and dominate the dynamics at high concentrations. The three-dimensional circulatory motion observed in our experiments above a critical film thickness can be interpreted as an interplay of two effects: expulsion of dense bacterial "clogs" into the depletion zone due to intrinsic chaotic fluctuations and their consequent slow motion in the depletion zone due to gravity and advection.

IV. STEADY-STATE CONCENTRATION DISTRIBUTIONS

To address the experimental situation and to develop a simplified qualitative description of the mixing and transport at high concentrations, we assume that the main effect of collective swimming is accounted in renormalized diffusivities for oxygen and bacteria D_c, D_n, while Eqs. (2) and (3) remain valid for steady-state vertical profiles of $n(z), c(z)$. This assumption is similar to the approximation of "turbulent viscosity" in the theory of hydrodynamic turbulence, where chaotic motion of the fluid is described by increased dissipation. Our assumption is further justified by comparison with experiment.

In the absence of an explicit fluid velocity field (here we assume that the large-scale motion of bacteria is absorbed in the diffusion coefficients, so in the steady state $\mathbf{u}=0$), the steady-state stationary vertical distributions of bacteria $n(z)$ and oxygen $c(z)$ can be obtained analytically. Integration of Eq. (3) yields $n = N \exp(\mu c / D_n)$, $N=$const. Eliminating n from Eq. (2), we obtain a simple equation for the oxygen concentration $c_{zz} - (Nk/D_c)\exp(\mu c / D_n) = 0$. This can be solved to yield the spatial distribution (4).

The thickness of depletion layer ξ is found from matching solutions of Eq. (4) with two different values of diffusivities, $D_{n1} \approx D_{c1} \approx 2.5-5 \times 10^{-5}$ cm^2/s outside the depletion zone and smaller values $D_n \approx 5 \times 10^{-6}$ cm^2/s, $D_{c1} \approx 2.1 \times 10^{-5}$ cm^2/s inside, with

$$n = n_{1,2} \sec^2 \left(\frac{z - d/2}{\lambda_{1,2}} \right), \qquad (6)$$

where $n_{1,2}$ are unknown concentration parameters determined from the matching and $\lambda_{1,2} = \sqrt{2 D_{n1,2} D_{c1,2} / \mu k n_{1,2}}$ are corresponding mixing lengths. The concentration parameters $n_{1,2}$ are obtained from the continuity of solution at the matching point $n(z) = n_{th}$ subject to total concentration conservation constraint $\int_0^d n(z) dz = \bar{n} d$. The total concentration constraint and the continuity condition give rise to the following equations:

$$\frac{\bar{n} d}{2} = n_1 \lambda_1 \left[\tan \left(\frac{d}{2\lambda_1} \right) - \tan \left(\frac{\xi}{2\lambda_1} \right) \right] + n_2 \lambda_2 \tan \left(\frac{\xi}{2\lambda_2} \right),$$

$$n_{th} = n_1 \sec^2 \left(\frac{\xi}{2\lambda_1} \right) = n_2 \sec^2 \left(\frac{\xi}{2\lambda_2} \right). \qquad (7)$$

The derived dependence of ξ vs film thickness d is shown in the inset to Fig. 5(b) and is in a good agreement with experimental values.

V. CONCLUSIONS

A noninvasive scanning technique has revealed novel insights into the spatial structures and their time evolution in concentrated bacterial suspensions, including accurate measurements of quantities not previously accessible. We have shown that the self-organized collective flows of motile bacteria greatly increase mixing rates in dense suspensions, which is manifested by increased effective diffusivity of bacteria and oxygen. We may speculate that this enhanced mixing and transport of oxygen is useful for the survival of the bacterial colonies under harsh conditions. However, according to studies in Ref. [25], bioconvection does not produce a clear positive increase in the bacterial colony growth rate, so the role of enhanced mixing and transport could be more subtle.

Our noninvasive measurements revealed a fundamentally different mechanism for convection in concentrated suspensions of swimming bacteria. This mechanism is related to the onset of a depletion layer and of macroscopic fluctuations intrinsic to the self-organized chaotic coherent locomotion. It yields an onset for three-dimensional motion much earlier than that predicted by linear stability analysis of the steady-state concentration distribution in the theory of oxygen-driven bioconvection when the organized motion of bacteria is neglected [15]. One surprising outcome of our work is that the mixing and transport of oxygen and bacteria are described qualitatively and even quantitatively by simple equations for advection and diffusion valid for dilute suspensions, but with greatly increased diffusivities. This approach is similar to the concept of turbulent viscosity in the theory of hydrodynamic turbulence. However, in our situation, this approach is more successful because the self-organized motion of bacteria possesses a well-defined length scale [5,10] in contrast to the well-known scale invariance of high Reynolds number turbulence. Thus, this coarse-graining procedure is formally justified.

ACKNOWLEDGMENTS

[1] E. Ben-Jacob, I. Cohen, O. Shochet, I. Aranson, H. Levine, and L. Tsimring, Nature (London) **373**, 566 (1995).

[2] I. H. Riedel, K. Kruse, and J. Howard, Science **309**, 300 (2005).

[3] X.-L. Wu and A. Libchaber, Phys. Rev. Lett. **84**, 3017 (2000).

[4] T. J. Pedley and J. O. Kessler, Annu. Rev. Fluid Mech. **24**, 313 (1992).

[5] C. Dombrowski, L. Cisneros, S. Chatkaew, R. E. Goldstein, and J. O. Kessler, Phys. Rev. Lett. **93**, 098103 (2004).

[6] I. Tuval, L. Cisneros, C. Dombrowski, C. W. Wolgemuth, J. O. Kessler, and R. E. Goldstein, Proc. Natl. Acad. Sci. U.S.A. **102**, 2277 (2005).

[7] J. P. Hernandez-Ortiz, C. G. Stoltz, and M. D. Graham, Phys. Rev. Lett. **95**, 204501 (2005); P. T. Underhill, J. P. Hernandez-Ortiz, and M. D. Graham, *ibid.* **100**, 248101 (2008).

[8] D. Saintillan and M. J. Shelley, Phys. Rev. Lett. **99**, 058102 (2007); **100**, 178103 (2008); Phys. Fluids **20**, 123304 (2008).

[9] L. H. Cisneros, R. Cortez, C. Dombrowski, R. E. Goldstein, and J. O. Kessler, Exp. Fluids **43**, 737 (2007).

[10] A. Sokolov, I. S. Aranson, J. O. Kessler, and R. E. Goldstein, Phys. Rev. Lett. **98**, 158102 (2007).

[11] J. Toner and Y. Tu, Phys. Rev. Lett. **75**, 4326 (1995).

[12] T. Vicsek, A. Czirók, E. Ben-Jacob, I. Cohen, and O. Shochet, Phys. Rev. Lett. **75**, 1226 (1995).

[13] I. D. Couzin and J. Krause, Adv. Study Behav. **32**, 1 (2003).

[14] M. J. Kim and K. S. Breuer, Phys. Fluids **16**, L78 (2004).

[15] A. J. Hillesdon and T. J. Pedley, J. Fluid Mech. **324**, 223 (1996); A. M. Metcalfe and T. J. Pedley, *ibid.* **370**, 24 (1998).

[16] G. K. Batchelor, *The Theory of Homogeneous Turbulence* (Cambridge University Press, New York, 1982).

[17] D. Huang *et al.*, Science **254**, 1178 (1991).

[18] F. I. Feldchtein *et al.*, in *SPIE*, edited by V. V. Tuchin, J. A. Izatt, and J. G. Fujimoto (SPIE, Bellingham, WA, 2005), Vol. 5690, p. 349.

[19] S. R. Williams and A. P. Philipse, Phys. Rev. E **67**, 051301 (2003).

[20] See EPAPS Document No. E-PLEEE8-80-033909 for experimental movies. For more information on EPAPS, see http://www.aip.org/pubservs/epaps.html.

[21] A. P. Berke, L. Turner, H. C. Berg, and E. Lauga, Phys. Rev. Lett. **101**, 038102 (2008).

[22] A. Sokolov and I. S. Aranson (unpublished).

[23] G. I. Taylor, Proc. R. Soc. London, Ser. A **219**, 186 (1953); **223**, 446 (1954).

[24] B. M. Haines, I. S. Aranson, L. Berlyand, and D. A. Karpeev, Phys. Biol. **5**, 046003 (2008).

[25] I. M. Jánosi, A. Czirók, D. Silhavy, and A. Holczinger, Environ. Microbiol. **4**, 525 (2002).